CrossMark

Effect of glottic geometry on breathing: three-dimensional unsteady numerical simulation of respiration in a case with congenital glottic web

M. Kürşat Gökcan[1,4] · Erkan Günaydinoğlu[2] · D. Funda Kurtuluş[3]

Abstract Glottic obstruction is a major cause of dyspnea. Without understanding the normal function of the glottis in breathing, treating dyspnea does not restore normal physiology. Therefore, we designed a computational fluid dynamics (CFD) model that tested the respiratory cycle in larynges with normal glottis and congenital glottic web (CGW). A CGW case and a control subject (CC) were selected from the computed tomography (CT) archive. 3D computational models of the larynges with structured boundary layer were constructed from axial CT images after mesh refinement study. CFD analyses were based on the Reynolds-averaged Navier–Stokes approach. Incompressible flow solver (pressure-based) and SST k-w turbulence model were chosen for this study. To simulate a real-time breathing process, time varying flow rate boundary condition was derived from the spirometer of a healthy, non-smoking woman. Glottic areas were measured as 51.64 and 125.43 mm^2 for the CGW patient and CC, respectively. Time-dependent velocity contours and streamlines for the CC and CGW patient were drawn. The CC showed uniform flow, all through the inspiration and expiration phases. However, the CGW patient showed separation of flow at the glottis level, which caused areas of stagnation in the supraglottis (during expiration) and the subglottis and trachea (during inspiration). Specialized geometry of the normal larynx maintained uniform flow with low shear stress values on the wall even at high mass flow rates. Distortion of this geometry may cause obstruction of flow at multiple levels and, therefore, should be evaluated at multiple levels.

Keywords Airway obstruction · Respiratory physiological phenomena · Glottic web, congenital anterior · Computational fluid dynamics · Respiration disorders, analysis · Respiration disorders, physiopathology

Introduction

The larynx plays a key role in many functions, such as respiration, phonation, swallowing, protection of the lower airways, clearance of the lungs, and fixation of intrathoracic pressure. In humans, the function of the upper aerodigestive tract is considerably more complex, owing to a higher level of development in phonation. The lower respiratory tract has evolved as an offshoot of the digestive tract, first appearing in the lungfish as a simple muscle sphincter to protect the lungs from water [1]. However, the larynx is far from that simple sphincter that merely opens and closes [2]. Breathing is a very dynamic process that has to adapt air passage from several hundred milliliters during quiet respiration to several liters in a second during forced respiration. Therefore, shape and neuronal control is specified to overcome these diverse needs.

The utilization of computational fluid dynamics (CFD) for airflow studies has opened another era like stroboscopy did for understanding VF waveform dynamics. In our

✉ M. Kürşat Gökcan
gokcan@medicine.ankara.edu.tr

1 Otorhinolaryngology, Head and Neck Surgery Department, Ankara University Medical School, Ankara, Turkey

2 Department of Flight Training, University of Turkish Aeronautical Association, Ankara, Turkey

3 Department of Aerospace Engineering, Faculty of Engineering, Middle East Technical University, Ankara, Turkey

4 Kehribar Sokak, Mesa Yamac 1 Sitesi 11A/12, GOP, Cankaya, Ankara, Turkey

 Springer

previous study, we utilized CFD for testing the efficacy of posterior transverse laser cordotomy in the treatment of bilateral abductor vocal fold immobility, and we found that the cross-sectional glottic area (GA) was not the only determinant of airflow. Our CFD experiments revealed that alterations of the three-dimensional laryngeal shape in paralyzed larynges and the shape of the glottic opening itself were as important as the dimension of the glottic opening in determining airflow [3]. One of the major shortcomings of that study was that we assumed a constant rate of airflow during inspiration. However, breathing is a very dynamic process where the rate and direction of flow changes in a few seconds. Thus, this study aimed to design a computational model that tests the whole respiratory cycle in a larynx where only the cross-sectional GA is diminished without any problem in laryngeal innervation.

Respiratory data from a spirometer were used to simulate unsteady airflow through the larynges of a patient with congenital glottic web (CGW) and a control case (CC) with a normal larynx. Spirometer measurement of a healthy volunteer was employed to simulate forceful, rapid breathing cycle to reveal aerodynamic events better in the

laryngeal conduit. Therefore, we planned to reach one step closer to the ideal computerized larynx model, where one can also put the aeroelastic properties and laryngeal movements into the testing environment.

Materials and methods

Study and control case selection

A retrospective chart review of CGW patients at our institution was performed, and the case of an 18-year-old adolescent female patient with CGW was selected. The case was the product of a term pregnancy without complications. Hoarseness and dyspnea on exertion had been her major complaint since infancy. Videolaryngoscopy revealed an anterior laryngeal web blocking about 50 % of the glottal area. Multidetector-computed tomography (MDCT) (Aquilion 64; Toshiba Medical Systems, Tokyo, Japan) was utilized (0.5-mm slice thickness and 0.5-mm reconstruction intervals), and virtual endoscopy was performed (Fig. 1). A thick web at the anterior portion extending into subglottis

Fig. 1 Virtual laryngoscopy and computational fluid dynamics mesh at the glottis section for **a** control case and **b** study case with congenital glottic web
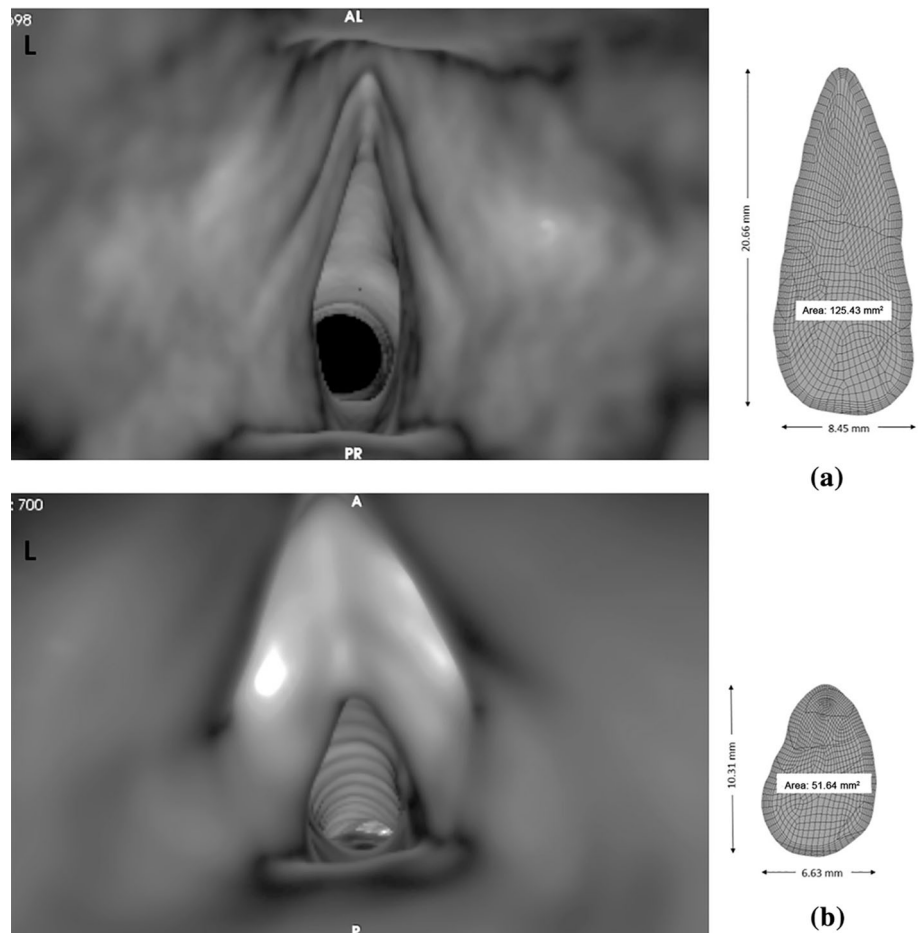
was seen. Patient was treated with endoscopic CO_2 laser vaporization of the web with topical mitomycin-C application. Her voice was weak but better than before, and her breathing was significantly improved in the early postoperative period. Patient defined mild level of dysphonia with relief in respiratory symptoms at the third postoperative month. An adult female CC was selected from MDCT archive (Fig. 1), who had MDCT for a reason other than imaging of the airway (neck vertebrate imaging).

Construction of the airway model

At the core of any CFD calculation is a computational grid, which is used to divide the solution domain into thousands or millions of elements in which the problem variables are computed and stored. To reconstruct a three-dimensional (3D) accurate model of studied larynges, axial MDCT sections of selected cases from the level of laryngeal inlet to the sixth tracheal ring were converted into uncompressed, lossless, 512×512 pixels tagged image file format (TIFF) image files. For the sake of precision, the pharyngeal airspace was excluded from the 3D model; therefore, the tip of the arytenoid plane was selected as the laryngeal inlet level. The TIFF images were read into the MATLAB code, and airway coordinates and boundaries were converted into two-dimensional (2D) splines that were 0.5 mm in thickness. The coordinates of the airway boundaries were used as input to the commercial mesh generator software (Gambit 2.4.6; ANSYS Inc., Canonsburg, PA, USA) to form an interlocking network throughout the volume where a planar surface could be generated and fluid flow analysis would take place. A similar procedure has been tested, applied, and explained in detail in our previous study [3].

To perform CFD analysis, computational domains representing the airway geometries should be divided into number of elements, where Navier–Stokes equations are solved. A structured boundary layer was used close to the wall region, and hexahedral grid type was chosen as the mesh type. Element numbers for CC and CGW patients were 133,920 and 112,203, respectively. A mesh refinement study was carried out for both models. Three different mesh types with element numbers 68,673 (coarse mesh), 133,920 (medium mesh), and 432,566 (fine mesh) were constructed for the CC. The medium mesh was selected, since mass flow rate differences between medium and fine meshes were less than 1 %, and also the computational time needed for the fine mesh configuration was extremely high. The same mesh refinement procedure was applied to the CGW patient. The results for medium mesh were obtained for six periods in 12 h in a 32-core 3.0-GHz CPU workstation. The results during the sixth period were presented in the current simulations where quasi-periodic solutions were obtained.

ANSYS Fluent 14.0 software (ANSYS Inc., Canonsburg, PA, USA) was used for transient CFD analysis, which was based on the Reynolds-averaged Navier–Stokes (RANS) approach. Incompressible flow solver (Pressure based) and SST k-w turbulence model was chosen for this study. The time step was varied during the simulation using a user-defined function from 0.005 s, except for the steep flow region between 0.67 s and 0.69 s, where the time step was decreased to 0.0001 s.

Clinical and boundary conditions

The boundary condition that was used in numerical analysis was derived from the spirometer results of an 18-year-old, healthy, non-smoking female volunteer, who was unrelated to test subjects. The same test conditions were applied for the simulations of both the CGW patient and the CC. To simulate a real-time breathing process, time varying flow rate boundary condition was defined at the exit of the simulation model (tracheal end) for modeling inspiration and expiration processes.

Spirometry was performed using a closed-circuit spirometry device (Spire™, ZAN Messgerate GmbH, Germany). The subject was asked to sit upright in a chair, breathe normally for 2–3 breaths before test, breathe in completely and rapidly, pause for less than 1 s, and exhale air as fast and as far as possible until completely empty or until unable to blow any longer [4]. The spirometer provided two graphics: (1) volume flow rate (l/s) versus volume graphics during expiration and inspiration (Fig. 2a) and (2) volume versus time (s) graphics during expiration (Fig. 2b) [4]. Print out graphics from the device were digitized as a TIFF file with a commercial scanner, and x–y coordinates were captured using a software (XYit Image Digitizer, Geomatix Ltd, UK) to create the numerical data file of the graphics.

Inspiration–expiration time is not provided in standard spirometry; therefore, inspiration time was obtained using a stopwatch during the spirometry test, and measured as 0.68 s for the volunteered subject. Expiration time was calculated from volume versus time graphics of expiration, with respect to the fact that the inspiratory reserve volume should be equal to the expiratory reserve volume according to the conservation of mass principle. This time was calculated as 4.12 s, and the data were also found to be in good agreement with the volume versus time graph obtained from the spirometer data (Fig. 2b) where the volume versus time graph converges to a constant vital capacity. The total time period of the inspiration–expiration was calculated as 4.8 s. Using measurements from the stopwatch and spirometry, a graph of volume flow rate (l/s) versus time (s) was drawn (Fig. 2c). User-defined function was defined at the exit of the flow domain for simulating transient flow condition.

Fig. 2 Estimation of boundary conditions from spirometer data: **a** volume flow rate versus volume, **b** volume versus time graphics during expiration, and **c** volume flow rate versus time graphics
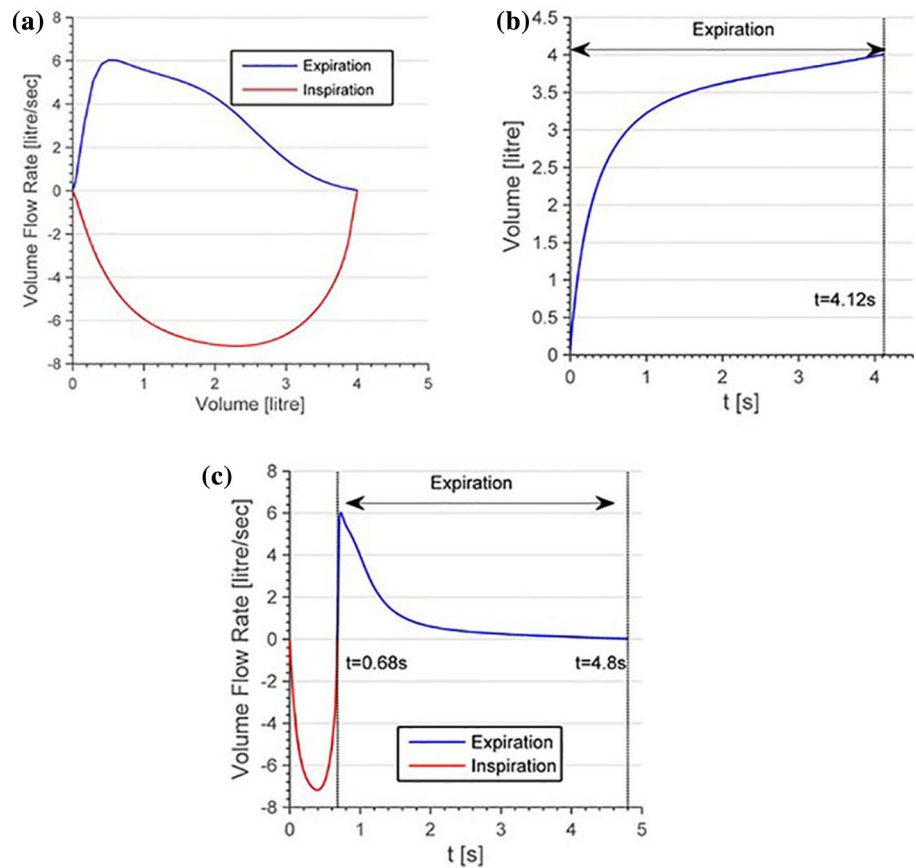
Time-dependent volume flow rate values were converted into mass flow rate by multiplying the data given in Fig. 2c by the density of air at 20 °C ($\rho = 1.225$ kg/m^3).

Results

The numerical simulations were compared for the CC and CGW patient at different time instances. The flow fields were represented at ten different plane cuts of the airways for both the CC and the CGW patient. These plane cuts are shown in Fig. 3. The locations of the inlet, glottis, and exit stations for both cases were adjusted to be at the same z-coordinate point. The glottis was at $z = 0$ location for both cases. As shown in Figs. 1 and 3, the cross-sectional areas through the larynx differed between the CC and CGW patient, especially at the glottis section. The GAs were measured as 51.64 and 125.43 mm^2 for CGW patient and CC, respectively.

Simulation of respiration for the CC and CGW patient

As shown in Fig. 2c, the inspiration process started at $t = 0$ and ended at $t = 0.68$ s, and the expiration started from
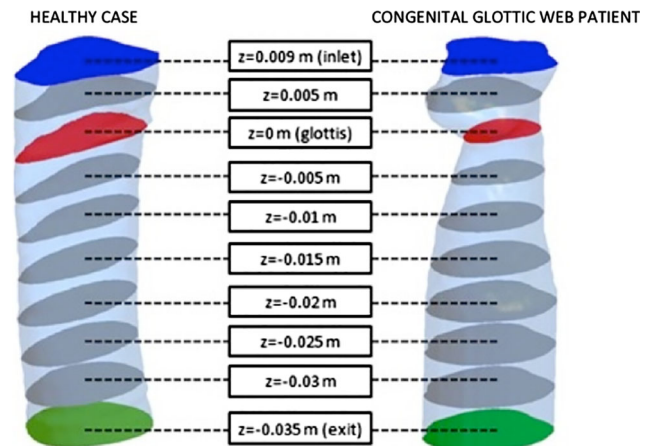

Fig. 3 Comparison of the geometries used for computational fluid dynamics experiments and cross sections where the results are presented

$t = 0.68$ s and ended at $t = 4.8$ s. The maximum volume flow rate of -7.18 l/s and mass flow rate of -8.8×10^{-3} kg/s were obtained at $t = 0.39$ s during inspiration. The maximum volume flow rate of 6.03 l/s and maximum mass flow rate of 7.39×10^{-3} kg/s values were calculated at $t = 0.72$ s during expiration.

The time-dependent velocity contours and streamlines for CC and CGW patient during inspiration and expiration phases are shown in Figs. 4 and 5, respectively. The w velocity was positive when the flow was from the lungs toward the laryngeal inlet, and the w velocity was negative when the flow was in the opposite direction (from laryngeal inlet toward the lungs).

At $t = 0.06$ s, just after the inspiration phase started, where the mass flow rate was very close to zero, a reverse flow was also observed at the posterior part of the glottis for the CGW patient (Fig. 4). This event disappeared very quickly and was the result of low velocities during which the air flow direction changed from expiration to inspiration. After inspiration started, the mass flow rate increased suddenly and reached its peak value of $\dot{m} = -0.0088$ kg/s (volume flow rate of -7.18 l/s) in a very short time. The peak flow rate value for inspiration was reached at $t = 0.39$ s. The flow rate decreased after its peak until the end of inspiration, $t = 0.68$ s.

The CC showed uniform flow all over the examined section of the larynx and trachea, throughout the inspiration phase. However, the CGW patient showed a growing number of recirculation zones at the subglottic area and trachea, causing air to leak from a smaller area at the posterior side of the subglottis and trachea. At the beginning of the inspiration phase (Fig. 4, $t = 0.06$ s), it was seen that the recirculation zone covered almost the entire trachea from the subglottic plane ($z = -0.01$ m) to the exit. The vortex structure grew as the mass flow rate increased. This recirculation zone was observed throughout the inspiration phase. There was also a smaller recirculation zone observed above the web area of the CGW patient, which was due to the rapid change in cross-sectional area.
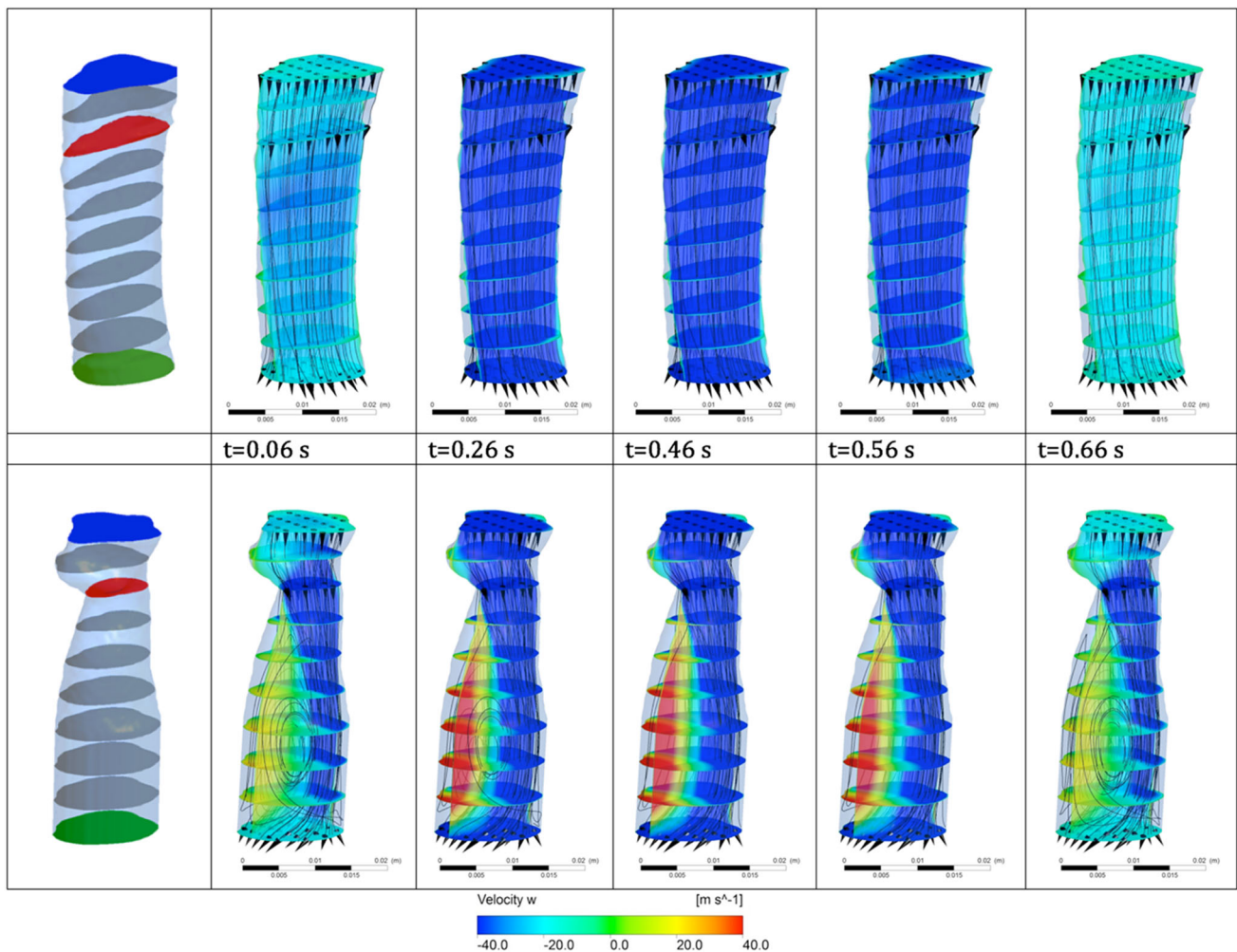

Fig. 4 Velocity contours and streamlines during inspiration phase for control case (CC; *first row*) and patient with congenital glottic web (CGW; *second row*)
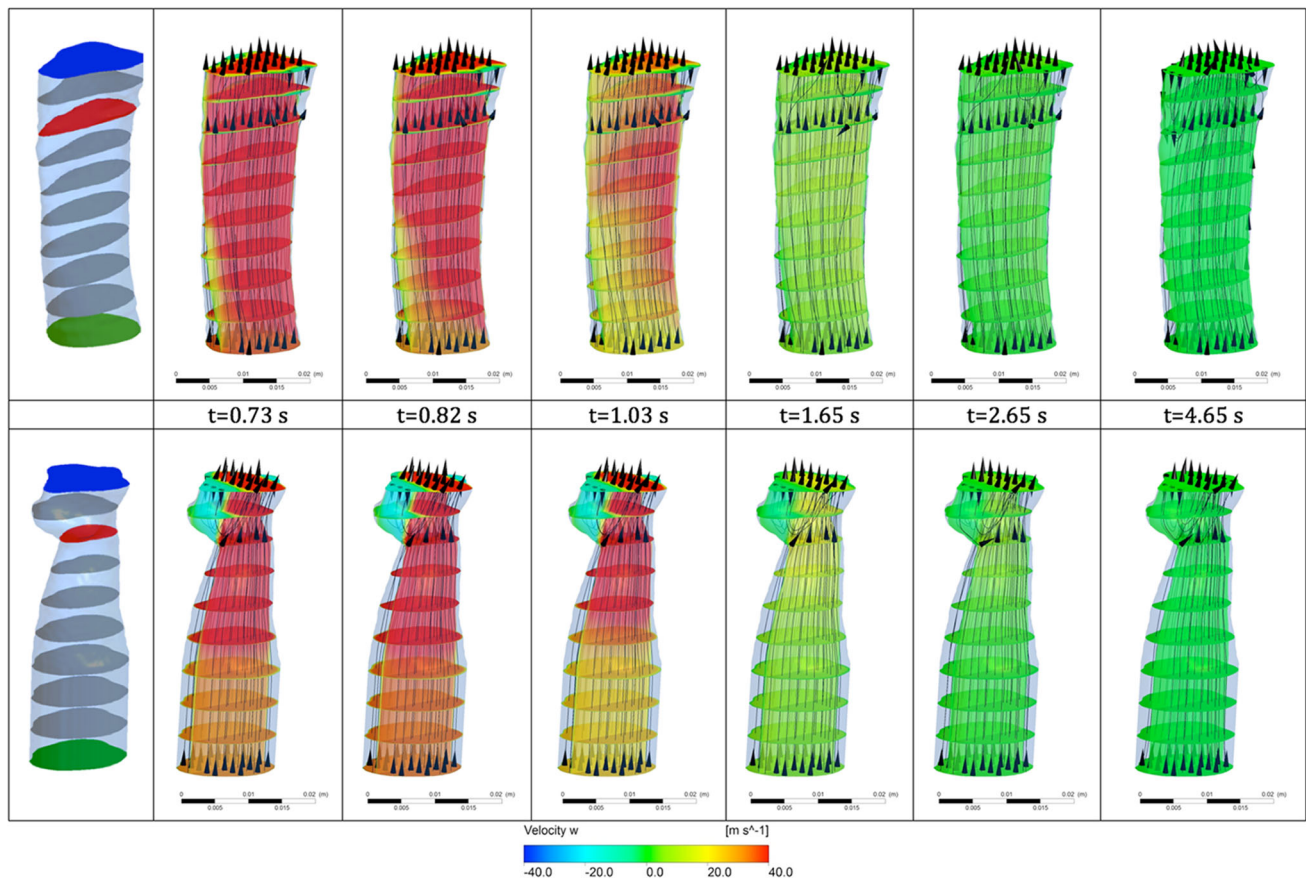
Fig. 5 Velocity contours and streamlines during expiration phase for control case (CC; *first row*) and patient with congenital glottic web (CGW; *second row*)

During expiration, it was observed that the flow was almost uniform and no separation of flow from the boundary layer [flow separation (FS)] was observed until the end of the expiration phase for CC (Fig. 5), except a small region at the back of the glottis. From $t = 0.72$ s, until the end of expiration, the mass flow rate and velocity decreased, and it was observed that the recirculation zone at the supraglottis of CC still remained the same with the decrease in the mass flow rate. The recirculation zone disappeared before start of the inspiration phase. However, for the CGW patient, the phenomenon of FS was observed throughout the expiration phase, leading to the formation of reverse flow areas mainly at the anterior part of the supraglottis due to recirculation zones. This reverse flow increased its intensity at the beginning of the expiration phase around the peak mass flow rates (blue region in Fig. 4, $t = 0.73$ s–1.03 s). This resulted in obstruction and decreased effective area usage at the laryngeal inlet for the CGW patient throughout the expiration period.

Decrease in GA led the velocities at the glottis to increase. The maximum velocity magnitude at the glottis has been calculated as 67 m/s for the CC and 137 m/s for the CGW patient.

Effectiveness of respiration

All objects exposed to a moving fluid acquire a boundary layer of fluid around them where viscous forces occur in the layer of fluid close to the solid surface. As it is seen from the total area distributions in Fig. 6, the laryngeal airway shape of a normal human looks like a convergent–divergent nozzle: the cross-sectional area gradually gets smaller from the inlet to the glottis, and then gets larger from the glottis to the trachea. The normal larynx maintained uniform flow even in forced respiration due to its special 3D shape. This shape directs air to the glottis during inspiration and expiration and prevents FS. However, changes in the glottic geometry in CGW cause a steep decline in the cross-sectional area and separation of flow from the boundary layer. The resultant vortex structures clog the airflow and cause stagnation areas or reverse flows throughout inspiration and expiration.
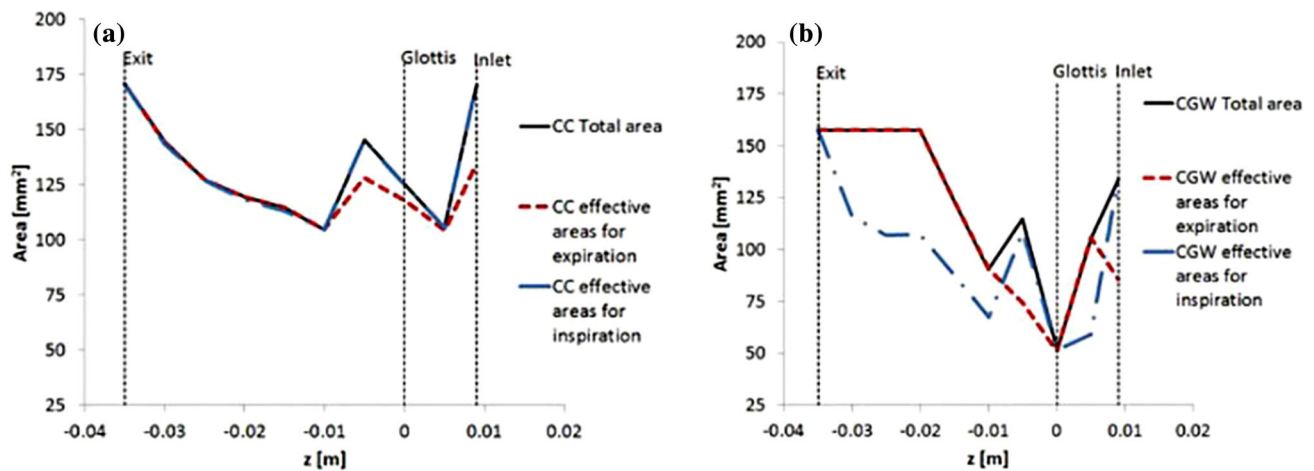
Fig. 6 Distribution of total area and minimum effective area measurements at supraglottis, glottis and trachea planes for the **a** CC and **b** CGW patient. The areas at the cross section where the flow is positive and where the flow is negative are calculated during the whole inspiration and expiration period for both the CC and CGW patients. *Solid lines* correspond to the real airway area at the given cross section. *Dashed lines* are the effective areas during inspiration (*blue*) and expiration (*red*)

The stagnation areas and reverse flow areas were subtracted from the total cross-sectional areas to obtain the effective areas used by the cases for both inspiration and expiration processes. Table 1 shows the measurement of cross-sectional areas and effective areas during inspiration and expiration for the CC and CGW patient, and Fig. 6 shows the distribution of the total areas and minimum effective areas. It is evident that the effectiveness ratio drops up to 56 % in the CGW patient. The CC uses her larynx with 100 % efficiency during most of the breathing, except during a small period during transition from expiration to inspiration.

Geometrical basis of effective respiration

Wall shear stress (WSS) is the force that acts tangential to the surface due to friction. Figure 7 compares the sagittal and coronal sections of larynges of the CC and CGW patient, and shows the distribution of total WSS from exit to inlet according to change in tangential angles. WSS for both cases was measured at $t = 0.46$ s (volume flow rate of -7 l/s), which was very close to the maximum flow rate at $t = 0.39$ s (volume flow rate of -7.18 l/s) during inspiration. For CC, the WSS values were observed very close to zero, both in the coronal and sagittal sections, all along the studied airway segment. However, the CGW case showed rapid increase in WSS in both planes when the distortion in the shape of larynx started. Therefore, the specialized shape of the normal larynx helped determining uniform flow with low shear stress values on the wall; even in high mass flow rates.

Discussion

In this study, we aimed to simulate airflow in a model where only glottis geometry was disturbed and compare it with a normal larynx model in an effort to reveal the influence of laryngeal structures on effectiveness of airflow. In addition, majority of the computational studies on human airway assume steady airflow; however, respiration is a dynamic process where the air volume changes according to physiological needs. Therefore, we applied unsteady airflow data obtained from the experimental spirometer measurements for real-like simulation of a forced respiration.

To the best of our knowledge, this is the first study in the literature to apply volumetric flow rate data with time. Majority of flow studies through the larynx assume the two-dimensional conduit and run experiments at a constant flow rate during inspiration or expiration. This study utilized real-time airflow data from a spirometer graph in a fine 3D computational model. Our data showed that the normal larynx maintained uniform flow and did not show any recirculation region throughout the inspiration and expiration phases. In addition, the specialized geometry of the larynx maintained the WSS close to zero, even in peak flow, and therefore increased respiratory efficiency (Fig. 7). WSS represents a measure of the forces exerted tangential to the luminal surface of the airway [5]. Laminar flow exerts a minimum force on the airway wall interface by developing a stable boundary layer between the primary stream of flow and the airway wall. Turbulent flow disrupts this boundary layer, generating greater shear stress values [5].

Table 1 Effective areas and effectiveness ratios for the congenital glottic web patient (CGW) and control case (CC)

Plane name	Exit							Glottis		Inlet
z (m)	−0.035	−0.03	−0.025	−0.02	−0.015	−0.01	−0.005	0	0.005	0.009
Area (CC) (mm²)	170.9	144.63	127.34	119.5	114.71	104.68	145.23	125.43	105.56	170.49
Area (CGW) (mm²)	157.58	157.52	157.53	157.53	123.05	90.42	114.66	51.64	105.56	134
Minimum effective area (CC) (mm²)	Expiration									
	170.9 (all the time)	144.45 (t = 1.03 s)	127.34 (all the time)	119.5 (all the time)	114.71 (all the time)	104.68 (all the time)	128.34 (t = 4.65 s)	117.7	104.24	134.3
	Inspiration									
	170.9 (all the time)	142.3 (t = 0.66 s)	126.95 (t = 0.26 s)	117.8 (t = 0.66 s)	112.9 (t = 0.66 s)	104.45	145.23 (all the time)	124.74	105.56 (all the time)	170.49 (all the time)
Minimum effective area (CGW) (mm²)	Expiration									
	157.58 (all the time)	157.52 (all the time)	157.53 (all the time)	157.53 (all the time)	123.05 (all the time)	90.42 (all the time)	74.2 (all the time)	51.3 (t = 2.65 s)	105.56 (all the time)	85.8 (t = 4.65 s)
	Inspiration									
	157.58 (all the time)	114.5 (t = 0.66 s)	106.9 (t = 0.66 s)	107.3 (t = 0.66 s)	87.13 (t = 0.66 s)	67.39 (t = 0.66 s)	108.4 (t = 0.66 s)	51.64 (all the time)	58.9 (t = 0.66 s)	134 (all the time)
Minimum effectiveness (CC) (%)	100	98	100	99	98	100	88	94	99	79
Minimum effectiveness (CGW) (%)	100	73	68	68	71	75	65	99	56	64

This geometry is specialized in three levels: (1) supraglottis, (2) glottis, and (3) subglottis. Hundertmark-Zauskova et al. performed a number of two-dimensional CFD experiments to find the optimal geometry of the larynx in terms of ease of breathing after the surgical change of VFs or false vocal folds (FVFs) [6]. They simulated airflow through the coronal cut plane of the normal larynx, and used that data to estimate the ideal position and thickness of VFs and FVFs after unilateral VF paralysis. Despite not reflecting real laryngeal shape and flow conditions, their experiments showed that airflow resistance and volumetric flow rate was affected by the distance between FVFs [6]. Our experiments revealed that FVFs act mainly during inspiration to direct air into a more uniform flow. The supraglottis functions to direct air to a narrower area, the glottis, during inspiration (Figs. 4, 7). Normally, when liquids are forced to flow in a narrower lumen, one can expect an increase in flow velocity and suction pressures behind, which may lead to FS after some level. Normal larynx showed uniform flow from the inlet (170 mm^2), through the glottis (125 mm^2), to the trachea (171 mm^2) without any FS, even at the peak of the inspiratory flow. Details of this 3D organization and results of its disturbance, as in the CGW case here, are given in the "Results" section in detail.

Role of the subglottic and glottic shape and structure on phonation has been studied in detail before [7, 8], but our literature search on their role in breathing did not show any result. FS is an important event in phonation; however, it decreases efficiency in respiration [7, 8]. The glottis has a converging effect on airflow during expiration, but a divergent effect during phonation [8]. Khosla et al. ran a series of experiments in excised canine larynges to reveal the aerodynamics (velocity fields) and the geometry of the medial surface of the vocal folds during the closing phase of vibration [8]. They obtained velocity field by use of a particle image velocimetry and measure pressure by use of a microphone and pressure transducer. Their work showed elegantly that FS vortices during phonation are closely related to the divergence angle, and subglottic pressure. As the divergence angle and subglottic pressure increased, FS vortices and resultant negative pressures above the superior half of the glottis increased, in their experiments. There was also skewing of the velocity waveform at mid to higher subglottal pressures, which caused an increase in the maximum flow declination rate and acoustic intensity. Our experiments showed that the conus elasticus acted mainly during expiration to maintain uniform flow, but FS was seen when the mass flow rate reduces. Therefore, we suggest that subglottic structures could be specialized mainly for phonation, although they also play a very important role during respiration. Combined with our results, these experiments are important to show that how the same geometry can adapt to increase both the efficiency of respiration and voice production [8].

Distortion in the three-dimensional relation in laryngeal structures caused higher level of obstruction from expected in CGW case: When we forced CGW case to breathe similar flow as a healthy individual, effective area dropped up to 56 % in the subglottis and 65 % in the supraglottis. This phenomenon was actually met, but could not be explained in many studies before. Saarinen et al. investigated airflow dynamics with spirometry and body plethysmography after VF augmentation in unilateral VF paralysis [9]. They found that medialization caused a decrease in the peak inspiratory flow. However, Cormier et al. found improved maximal expiratory flow after intracordal Teflon injection [10]. Some other studies also reported some levels of change in spirometer parameters after vocal fold medialization, although patients rejected any level of dyspnea after surgery [11]. Therefore, these studies showed a change in the airflow due to VF paralysis or medialization, but were unable to relate this finding to the distortion in 3D laryngeal geometry.

The main shortcomings of our study are that our CFD models assumed rigid walls, and neglected the upper and lower airways. Clinical observations and experimental evidence indicate that the larynx and vocal folds may move actively during respiration [1, 2]. Therefore, we cannot estimate the influence of neuronal control during forced respiration and the effect of nasal and pharyngeal anatomy on airflow. In addition, retrospective nature of the study hinders us from estimating the possible influence of anthropometric variability of subjects on our calculations. Neck fat tissue distribution is related to body weight and height and has been shown to effect retroglossal and retropalatal airway volume [12]. However, normative data of laryngotracheal dimensions and shape are shown to be related to age (as being an adult or child) and sex [13]. We chose a CC from the same gender with CGW case, as we are studying in laryngeal conduit that has a cartilage skeleton. Body height and weight should have negligible effect on laryngeal conduit, if any.

The results are derived using the laryngeal geometry of a single case and a control. CFD experiments can be quite time-consuming depending on the method of 3D model construction, mesh generation, grid number, time increment, and the processing capacity of the computer environment. We did not use commercial image-based engineering programs to build 3D models, which might decrease model generation time. Six cycles of time varying simulation of respiration, in a 133,920 node mesh, took around 12 h with a 32-core, 3.0-GHz CPU workstation. Specialization in fluid dynamics is required during mesh generation and parameter selections for CFD software. Therefore, further experience and development in

CORONAL SECTION
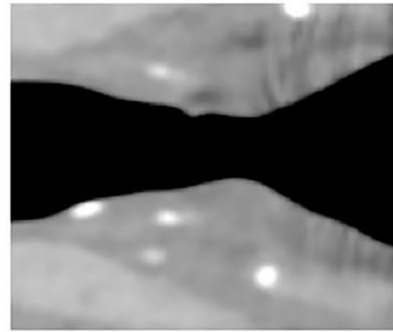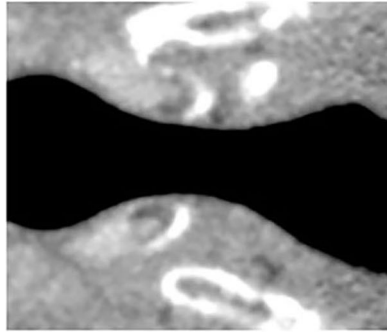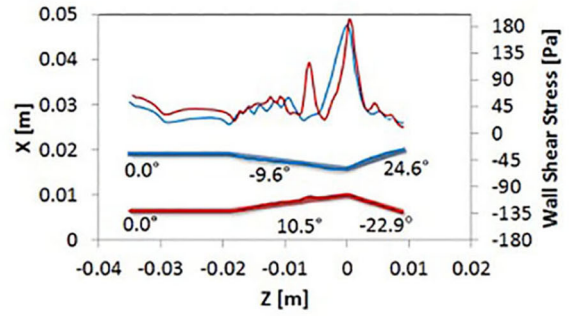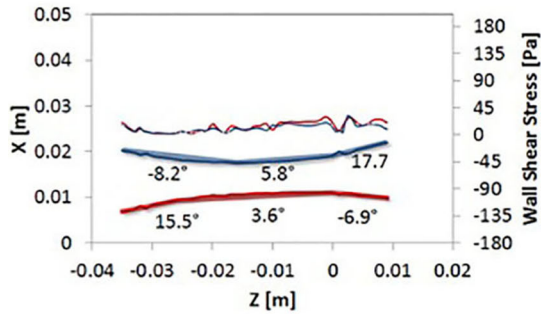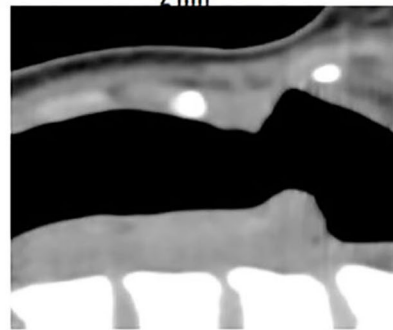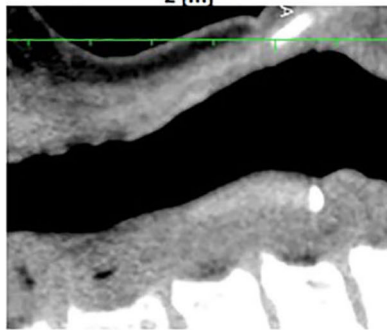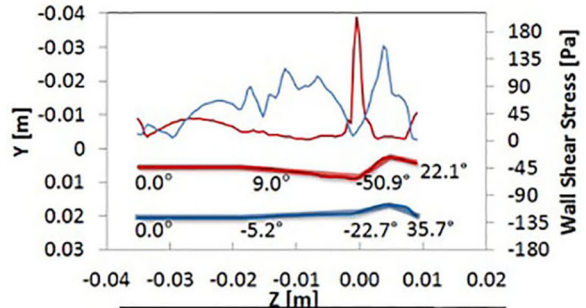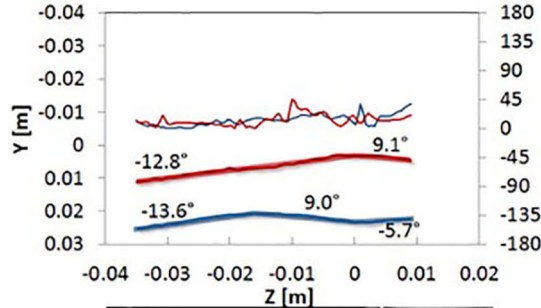
SAGITTAL SECTION

◄ **Fig. 7** Comparison of laryngeal geometries of the CC and CGW patients in coronal and sagittal sections with distribution of maximum wall shear stress values at $t = 0.46$ s. In the sagittal section, CC has almost a constant contour with 0.8° divergence from exit until $x = -0.0016$ m angle [−12.8° to (−13.6°) = 0.8°]. After this almost constant contour, the normal larynx shows a divergence of 21.9° at the subglottic level till the anterior commissure (from $x = -0.0016$ m to 0 m; −12.8° to 9.0° = −21.9°). The glottis of the CC is observed to be a constant duct with almost zero angular difference (0.1°). This linear pipe behavior of the glottis is important to prevent separation of flow region results the uniform flow of the CC during the whole period of the simulation. From glottis to inlet 14.8° [9.1° to (−5.7°) = 14.8°], convergence is seen. The CGW patient, on the other hand, shows a convergence at the subglottic level with 14.2° angular difference due to subglottic extension of anterior glottic web. A very steep divergence angle of 28.1° was seen at the glottis region due to web formation. In the coronal section at the widest glottal opening, the normal larynx shows a smooth convergence of 23.7° and divergence of 26.4°. The glottis shows small divergence angle of 2.2°. The CGW patient, on the other hand, in the coronal section seems to have very strong angular change throughout the glottis. The convergence part has an angle of 20.1° between left and right walls, and after the glottis, this angular section suddenly becomes divergent with an angle of 47.5°, approximately twice as much as that seen in the normal patient. This jet flow and abrupt angular change in the geometry causes separation of airflow from boundary layer and resultant vortex formation

computer and software technology with validation of results are required until routine utilization of CFD calculations in the evaluation of dyspneic patient and/or surgical design.

Conclusion

A key contribution of this study is the description of the physical properties of the larynx as an organ of respiration. The computerized model helps us to illustrate the events when a subject breathes forcefully, as when during spirometry. Furthermore, it brings forward the phenomenon that the effective cross-sectional area of the flow conduit may be diminished due to separation of flow from the boundary layer and resultant vortex structures. We hope that this study will provide a new perspective in understanding and treating glottic obstruction. Therefore, we encourage researchers, including ourselves, to utilize and improve CFD models for providing better healthcare to patients with dyspnea.

Compliance with ethical standards

References

1. Negus V (1949) Comparative anatomy and physiology of the larynx. Heinemann, London
2. Woodson GE (2010) Laryngeal and pharyngeal function. In: Flint PW, Haughey BH, Lund VJ et al (eds) Cummings otolaryngology head and neck surgery, 5th edn. Mosby, Philadelphia, pp 805–812
3. Gökcan MK, Kurtuluş DF, Ustüner E et al (2010) A computational study on the characteristics of airflow in bilateral abductor vocal fold immobility. Laryngoscope 120:1808–1818. doi:10.1002/lary.21003
4. West JB (2008) Respiratory physiology: the essentials, 8th edn. Lippincott Williams & Wilkins, Philadelphia
5. Mihaescu M, Gutmark E, Murugappan S, Elluru R, Cohen A, Willging JP (2009) Modeling flow in a compromised pediatric airway breathing air and heliox. Laryngoscope 119:145–451. doi:10.1097/MLG.0b013e3181856051
6. Hundertmark-Zaušková A, Lehmann R, Hess M, Müller F (2013) Numerical simulation of glottal flow. Comput Biol Med 43:2177–2185. doi:10.1016/j.compbiomed.09.009
7. Fulcher LP, Scherer RC, Zhai G, Zhu Z (2006) Analytic representation of volume flow as a function of geometry and pressure in a static physical model of the glottis. J Voice 20:489–512. doi:10.1016/j.jvoice.2005.07.006
8. Khosla S, Oren L, Ying J, Gutmark E (2014) Direct simultaneous measurement of intraglottal geometry and velocity fields in excised larynges. Laryngoscope 124(Suppl 2):S1–S13. doi:10.1002/lary.24512
9. Saarinen A, Rihkanen H, Lehikoinen-Söderlund S, Sovijärvi AR (2000) Airway flow dynamics and voice acoustics after autologous fascia augmentation of paralyzed vocal fold. Ann Otol Rhinol Laryngol 109:563–567
10. Cormier Y, Kashima H, Summer W, Menkes H (1978) Airflow in unilateral vocal cord paralysis before and after Teflon injection. Thorax 33:57–61
11. Ejnell H, Månsson I, Bake B, Stenborg R (1984) Laryngeal obstruction after Teflon injection. Acta Otolaryngol 98:374–379
12. Shigeta Y, Enciso R, Ogawa T, Ikawa T, Clark GT (2008) Cervical CT derived neck fat tissue distribution differences in Japanese males and females and its effect on retroglossal and retropalatal airway volume. Oral Surg Oral Med Oral Pathol Oral Radiol Endod 106:275–284. doi:10.1016/j.tripleo.2008.03.024
13. Seo JH, Hwang SH, Kang JM, Kim CS, Joo YH (2014) Age-related changes of the larynx and trachea assessed by three-dimensional computed tomography in children: application to endotracheal intubation and bronchoscopy. Clin Anat 27:360–364. doi:10.1002/ca.22290